# Electronic Transparency Limit of hBN Separation Layer for Quantum-Hybridization Negative Differential Resistance in Vertical Graphene/hBN/Graphene Heterojunctions

Tae Hyung Kim
School of Electrical Engineering, Korea Advanced Institute of Science and Technology (KAIST)
Yuseong-gu, Daejeon, Korea
ramanujankim@kaist.ac.kr

Juho Lee
School of Electrical Engineering, Korea Advanced Institute of Science and Technology (KAIST)
Yuseong-gu, Daejeon, Korea
thinker0817@gmail.com

Yong-Hoon Kim
School of Electrical Engineering, Korea Advanced Institute of Science and Technology (KAIST)
Yuseong-gu, Daejeon, Korea
y.h.kim@kaist .ac.kr

***Abstract*—The negative differential resistance (NDR) phenomenon emerging from vertically stacked two-dimensional (2D) van der Waals (vdW) heterostructures consisting of few-layer hexagonal boron nitride (hBN) sandwiched by graphene (Gr) electrodes has been traditionally explained in terms of the semiclassical resonant tunneling. However, we recently showed that the alternative quantum-hybridization NDR (QH-NDR) mechanism can be effective with the defective hBN. Here, with the increasing bias voltage, the quantum mechanical hybridization between Gr and hBN defect states supports the increase of currents up to the NDR peak, at which the abrupt breaking of QH then leads to the NDR valley regime. This phenomenon was identified in the tree-layer hBN channel case with a defect positioned in the central layer, and the presence of pristine hBN monolayer (1L) separating Gr and defective hBN was found to be the precondition of obtaining the QH-NDR signal. Carrying out multi-space constrained-search density functional calculations, we examine the generality of this observation and in doing so deepen our understanding of the QH-NDR phenomena in Gr electrode-based 2D vdW heterojunctions. Specifically, we adopt the four-layer hBN channel model and consider various configurations of hBN defects. We observe that the defect-mediated QH-NDR signal appears as long as an hBN defect is separated from another hBN defect or Gr by pristine 1L hBN. These findings not only confirm the wide applicability of the QH-NDR mechanism but also could prove to be a useful guideline for the design of 2D vdW devices**

***Keywords—graphene, hBN, quantum hybridization, negative differential resistance, nonequilibrium first-principles calculations***

## I. INTRODUCTION

Conventional explanations of the quantum mechanical negative differential resistance (NDR) relied on the band-to-band tunneling in the tunnel diode or the resonant tunneling through double barriers in the resonant-tunneling diode [1]. However, in our recent study, utilizing one-dimensional (1D) van der Waals (vdW) halide perovskite nanowires, we established a novel quantum-hybridization NDR (QH-DNR) mechanism [2, 3]. This mechanism emerges from the initial quantum mechanical hybridization throughout the source-channel-drain regions and its breaking with the increasing applied bias voltage. We further extended the applicability of the QH-NDR mechanism to vertically stacked two-dimensional (2D) vdW heterojunctions. Specifically, by employing a tri-layer (3L) hBN channel sandwiched by Gr electrodes, we showed that the introduction of a carbon atom substituted for a nitrogen atom ($C_N$) within the central hBN layer can induce a symmetric NDR feature due to the QH-NDR principle (**Fig. 1a**) [4]. This QH-NDR mechanism in vertically stacked 2D Gr/few-layer hBN/Gr heterojunctions successfully explains the experimentally observed symmetric NDR curve [5], which cannot be accounted for based on the semiclassical tunneling mechanisms [6]. However, the generality and specific conditions for the emergence of the QH-NDR signals in 2D vdW heterojunctions still remain unexplored.

In this report, adopting the Gr/four-layer (4L) hBN/Gr heterojunction model (**Fig. 1b**), we confirm the generality of the QH-NDR mechanism in Gr-based 2D vdW heterojunctions and establish that the precondition of its emergence is the defective hBN layer being separated from the adjacent Gr or neighboring defective hBN layer by pristine single-layer (1L) hBN.

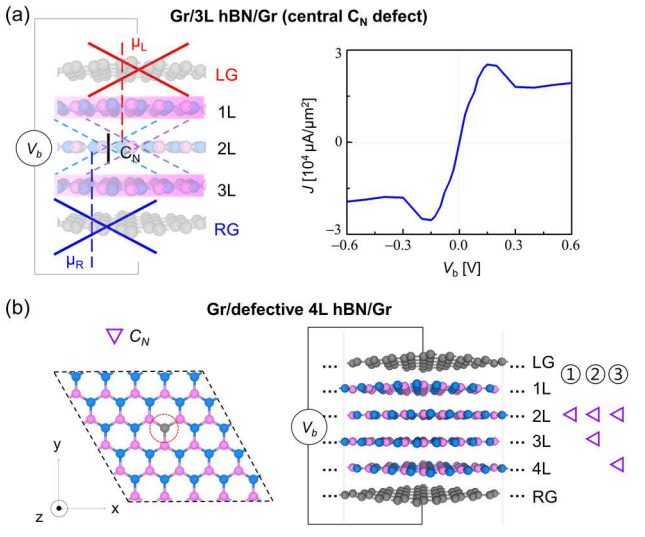


**Fig. 1.** (a) The schematics of QH-NDR mechanism in Gr/defective 3L hBN/Gr junction with the central $C_N$ defect (left) and corresponding $J - V_b$ characteristics (right). (b) The $C_N$ defect on the hBN layer (left) and Gr/defective 4L hBN/Gr junction model with three different cases of $C_N$ defect position (right).

## II. METHODS

*DFT and MS-DFT calculations*: All equilibrium density functional theory (DFT) and nonequilibrium multi-space constrained search DFT (MS-DFT) calculations [4, 7, 8] were performed using the SIESTA software package [9] within the LDA exchange-correlation functional [10]. The atomic cores were replaced by norm-conserving pseudopotentials of Troullier-Martins type [11], and the double $\zeta$-plus-polarization-level numerical atomic orbital basis sets were employed. For the Gr/defective 4L hBN/Gr heterojunctions, a 5×5 supercell of Gr/4L hBN/Gr model was adopted. For the defective hBN layer, one single $C_N$ defect was introduced into the supercell, which corresponds to the defect density of $7.63\times10^{13}$ cm$^{-2}$.

*MGF calculations*: After obtaining nonequilibrium electronic structures, the matrix Green's function (MGF) formalism was used for the post-processing step to obtain the electron transmissions, $T(E;V) = \mathrm{Tr}[\boldsymbol{\Gamma_L G \Gamma_R G^+}]$, where the $\boldsymbol{\Gamma_{L/R}}$ is the broadening matrices and $\boldsymbol{G}$ is the retarded Green's function for the channel region [12, 13]. The current was calculated using the Landauer-Buttiker formula [14],

$$J(V_b) = \frac{2e}{hW}\int_{\mu_L}^{\mu_R} T(E;V_b)[f(E-\mu_R) - f(E-\mu_L)]dE, \quad (1)$$

where $f(E-\mu) = 1/\{1+exp((E-\mu)/k_BT)\}$ is the Fermi-Dirac distribution function.

## III. RESULTS & DISCUSSION

Reminding that we previously observed in Gr/3L hBN/Gr heterojunctions the defect-mediated symmetric QH-NDR features only when the $C_N$ defect is located in the central hBN layer [4], we now discuss whether the QH-NDR signals appear in Gr/defective 4L hBN/Gr heterojunctions and if so the conditions for the emergence of QH-NDR. For the 4L hBN channel, we considered the three cases as indicated in **Fig. 1b**: ① one $C_N$ defect placed in the second hBN ($C_N^2$) layer, ② two $C_N$ defects placed in the second ($C_N^2$) and third hBN ($C_N^3$) layers, and ③ two $C_N$ defects placed in the second ($C_N^2$) and fourth hBN ($C_N^4$) layers. The current density-bias voltage ($J-V_b$) characteristics of the three models are shown in **Figs. 2a**, **Fig. 3a**, and **Fig. 4a**, respectively. We then find that, while the case ① does not exhibit an NDR signal, we obtain symmetric NDR signals from cases ② and ③. To analyze the origins for the absence or presence of NDR signals, and particularly explain that the NDR signals in cases ② and ③ results from the QH-NDR mechanism, we analyzed the electronic bands projected onto the left graphene (LG), right graphene (RG), and the hBN channel, as well as the real-space charge density differences between LG/RG and hBN

$$\delta\rho(\boldsymbol{r}) = \rho^{LG/hBN/RG}(\boldsymbol{r}) - \left[\rho^{LG/RG}(\boldsymbol{r}) + \rho^{hBN}(\boldsymbol{r})\right], \quad (2)$$

and the corresponding plane-averaged Hartree potential differences

$$\delta\bar{v}_H(\boldsymbol{z}) = \bar{v}_H^{LG/hBN/RG}(\boldsymbol{z}) - \left[\bar{v}_H^{LG/RG}(\boldsymbol{z}) + \bar{v}_H^{hBN}(\boldsymbol{z})\right]. \quad (3)$$

Note that while $\delta\rho$ and $\delta\bar{v}_H$ provide the electrostatic information the projected electronic bands reveal more detailed electronic structure information [15, 16].

For the case ①, we find in equilibrium an electron accumulation at the $C_N^2$ defect or the charge transfer from graphene to $C_N^2$, which induces an initial $p$-doping of both the LG and RG electrodes (**Fig. 2b**, top panel). The asymmetric character of charge transfers along the LG and RG directions apparently results in the misalignment of LG and RG Dirac cones with a positive built-in potential of +0.07 eV between LG and RG even at $V_b$ =0 V.

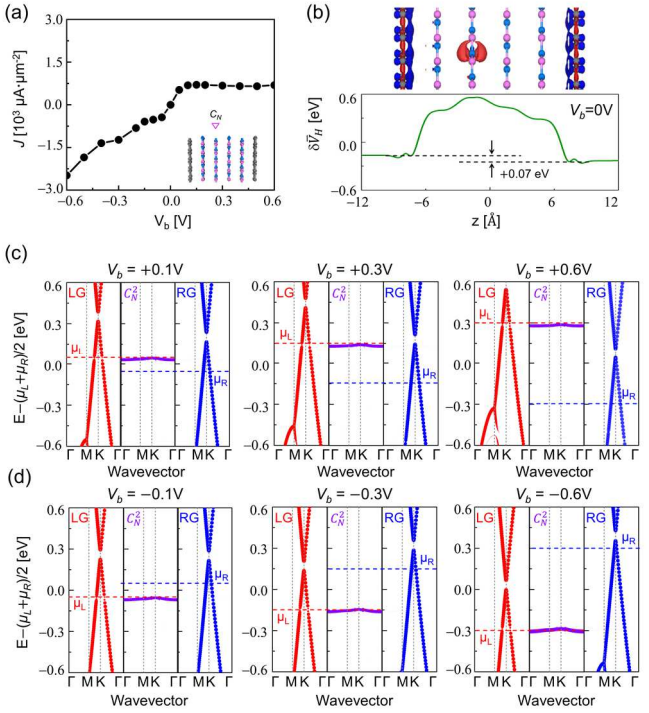


**Fig. 2.** (a) $J-V_b$ curves of Gr/defective 4L hBN/Gr junction with $C_N$ defects placed on second hBN layer (inset). (b) The $\delta\bar{v}_H$ profiles (green solid line) and the real-space $\delta\rho$ (overlaid inset) of the junction at the equilibrium condition. The red and blue colors indicate the electron accumulation and depletion, respectively. Here, the isosurface level is 0.0037 eÅ$^{-3}$. The projected band structures of LG (red circles), $C_N^2$ (purple circles), $C_N^4$ (orange circles), and RG (right circles) at (c) positive $V_b$ (+0.1 V, +0.3 V, +0.6 V) and (d) negative $V_b$ (−0.1 V, −0.3 V, and −0.6 V).

Next, we analyze the behavior of the projected bands of LG (red circles), RG (blue circles), and $C_N^2$ defect states (purple circles) with increasing $V_b$ (**Figs. 2c** and **2d**). We observe that the $C_N^2$ state moves together with the LG states with $V_b$ (**Figs. 2c** and **2d**), indicating the strong hybridization between the $C_N^2$ and LG states (or the pinning of $C_N^2$ states to LG states) across the 1L hBN separation. On the other hand, the $C_N^2$ /RG interface is separated by two hBN layers, apparently resulting in the disconnection between $C_N^2$ defect and RG electrode states.

Now, together with the initial asymmetric $p$-doping of the LG and RG electrodes, the strong pinning of $C_N^2$ to LG states explains the highly asymmetric $J-V_b$ characteristic: For the positive $V_b$ case, the hybridized $C_N^2$/LG states pass through the RG electrode Dirac point (**Fig. 2c**). Accordingly, the amount of RG states that match the $C_N^2$/LG states decreases with increasing $V_b$, which results in the $J$ that remains nearly constant as shown in **Fig. 2a**. On the other hand, for the negative $V_b$, the overlap between $C_N^2$/LG and RG states in the energy and momentum space gradually increases, allowing for the increased probability of electron tunneling from LG to RG electrode. Consequently, $J$ linearly increases with decreasing $V_b$, as shown in the negative $V_b$ regime of **Fig. 2a**.

In the case ② (**Fig. 3a**, inset), as mentioned earlier, we observe an NDR signal with the PVR of 6.25 (**Fig. 3a**). Similar to the case ①, the $C_N$ defects induce initial *p*-doping in the LG and RG electrodes due to the extraction of electrons from Gr electrodes. However, as shown in the bottom panel of **Fig. 3b**, we observe that the symmetric distribution of $C_N$ defects within the four hBN layers results in zero built-in potential across the junction model in equilibrium and the symmetric $J - V_b$ characteristics observed in **Fig. 3a**.

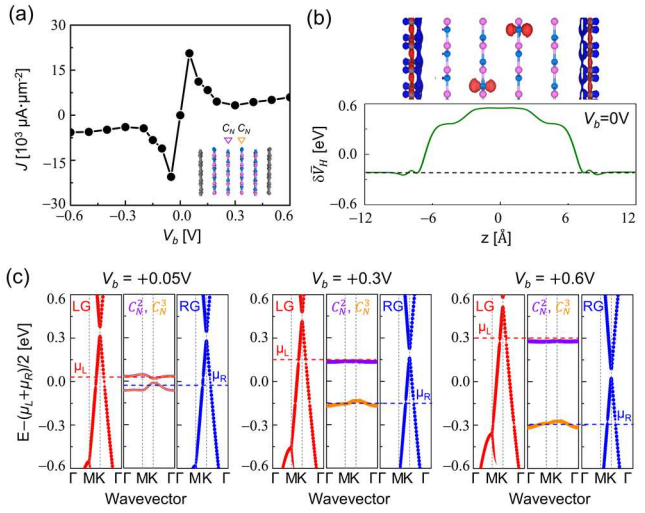


**Fig. 3.** (a) $J - V_b$ curves of Gr/defective 4L hBN/Gr junction with $C_N$ defects placed on second and third hBN layers (inset). (b) The $\delta\bar{v}_H$ profiles (green solid line) and the real-space δρ (overlaid inset) of the junction at the equilibrium condition. (c) The projected band structures of LG (red circles), $C_N^2$ (purple circles), $C_N^4$ (orange circles), and RG (right circles) at $V_b = +0.05$ V, +0.3 V, and +0.6 V.

In **Fig. 3c**, we also provide the projected bands at finite $V_b$. As presented in the left-second panel of **Fig. 3c**, the two defect states overlap with each other or the initial hybridization between $C_N^2$ (purple circles) and $C_N^3$ (orange circles) is maintained at $V_b = +0.05$ V. This defect-mediated strong hybridization across the entire Gr/4L hBN/Gr interface initially results in significant increase in $J$ (**Fig. 3a**). However, as $V_b$ increases further, the hybridization between $C_N^2$ and $C_N^3$ eventually breaks down, resulting in the QH-NDR behavior. After the disruption of $C_N^2/C_N^3$ hybridization, each defect level follows the adjacent Gr electrode with $V_b$, resulting in the independent upshift/downshift of the $C_N^2/C_N^3$ defect levels with increasing $V_b$ (**Fig. 3c**, middle and right panels). More specifically, as $V_b$ increases, the $C_N^2/C_N^3$ states are gradually occupied/depleted with the electrons being transferred from/to the LG/RG electrode.

We emphasize that once the defect levels are split, each defect level qualitatively behaves similarly to the case ① (**Fig. 2**), or each $C_N$ defect level becomes pinned to the adjacent Gr electrode across the 1L hBN (**Fig. 3c**, middle and right panels). This pinning of $C_N$ defect levels to adjacent Gr electrode levels impedes the coupling between LG and RG electrodes mediated by the two $C_N$ defect states, resulting in the reduction of the electron transport from LG to RG and leading to the valley regimes in the QH-NDR signal in **Fig. 3a**.

In the final case ③, we introduced two $C_N$ defects into the second ($C_N^2$) and fourth hBN ($C_N^4$) layers as shown in the inset of **Fig. 4a**. In this configuration, we again observe the NDR signal in both positive and negative $V_b$ regimes with the PVR of 7 at positive $V_b$ and the $J$ peak (valley) at $V_b = +0.2$ V (+0.5 V).

From the analysis of the $\delta\rho$ profiles in equilibrium (**Fig. 4b**, top panel), we also find that electrons are accumulated at both the $C_N^2$ and $C_N^4$ defects, leading to the initial *p*-doping of both LG and RG electrodes. Due to its proximity to the RG electrode, the $C_N^4$ defect exhibits larger electron accumulation at than the $C_N^2$ defect. The asymmetric electron accumulation at $C_N^2$ and $C_N^4$ defects then results in a minimal $\delta\bar{v}_H$ step of ~+0.02 eV (+ 0.03 eV) between the $C_N^2$ and $C_N^4$ defects (LG and RG electrodes) (**Fig. 4b**, bottom panel). This minute $d\bar{v}_H$ steps indicate that the $C_N^2$ and $C_N^4$ defects (defects-mediated LG and RG states) are hybridized in spite of the separation by 1L hBN between $C_N^2$ and $C_N^4$ (LG and $C_N^2$).

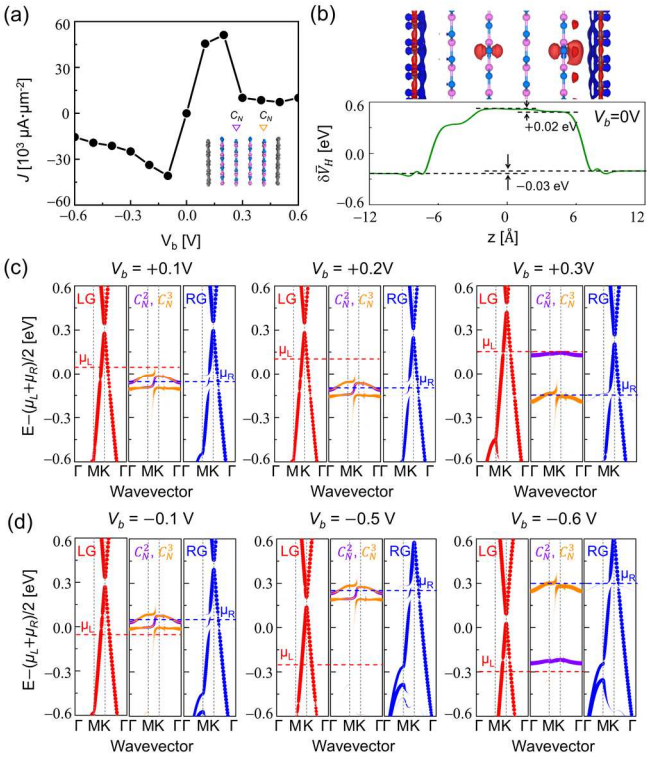


**Fig. 4.** (a) $J - V_b$ curves of Gr/defective 4L hBN/Gr junction with $C_N$ defects placed on second and fourth hBN layers (inset). (b) The $\delta\bar{v}_H$ profiles (green solid line) and the real-space $\delta\rho$ (overlaid inset) of the junction at the equilibrium condition. The projected band structures of LG (red circles), $C_N^2$ (purple circles), $C_N^4$ (orange circles), and RG (right circles) at (c) positive $V_b$ (+0.1 V, +0.2 V, +0.3 V) and (d) negative $V_b$ (−0.1 V, −0.5 V, and −0.6 V).

Analyzing the projected band structures shown in **Fig. 4c** (**Fig. 4c**), we find that the initial strong hybridization between the $C_N^2$ and $C_N^4$ defect states is maintained up to $V_b = +0.2$ V ($V_b = -0.5$ V) in the positive (negative) $V_b$ regime. In addition, the direct contact between $C_N^4$ and RG electrode results in the $C_N^4$/RG layers acting as a single entity and the pinning of $C_N^2$ defect states to the combined $C_N^4$ /RG "electrode" (**Figs. 4c** and **4d**, left and middle panels). However, as the $V_b$ further increases or decreases, the coupling between $C_N^2$ and $C_N^4$ states is abruptly broken, leading to the splitting of the two defect levels (**Figs. 4c** and **4d** right-second panels). The changes in the hybridization between $C_N^2$ defect and $C_N^4$/RG electrode states then lead to the decreases in the magnitude of $J$ values and the observed QH-NDR signals in **Fig. 4a**.

## IV. Conclusion

In summary, performing MS-DFT calculations, we systematically investigated the generality and preconditions for the activation of the QH-NDR mechanism in vertically stacked Gr/few-layer hBN/Gr 2D vdW heterojunctions. We established that the presence of a pristine 1L hBN separation facilitates the quantum hybridizations between Gr and defective hBN layer as well as between two defective hBN layers, generating QH-NDR features. However, once 2L hBN separate them, the NDR signal disappeared or Gr and defective hBN became electronically decoupled. Our findings provide valuable insights into the QH-NDR mechanism and more generally offer a guidance for the design of quantum-mechanical 2D devices.

## Acknowledgment

This work was supported by the Samsung Research Funding & Incubation Center of Samsung Electronics (No. SRFC-TA2003-01).

## References

[1] L. Esaki, "Long journey into tunneling," *Proceedings of the IEEE,* vol. 62, no. 6, pp. 825-831, 1974.

[2] M. E. Khan, J. Lee, S. Byeon, and Y.-H. Kim, "Semimetallicity and negative differential resistance from hybrid halide perovskite nanowires," *Adv. Funct. Mater.,* vol. 29, no. 13, p. 1807620, 2019.

[3] J. Lee, M. E. Khan, and Y. H. Kim, "Quantum hybridization negative differential resistance from non-toxic halide perovskite nanowire heterojunctions and its strain control," *Nano Converg,* vol. 9, no. 1, p. 25, Jun 1 2022.

[4] T. H. Kim, J. Lee, R.-G. Lee, and Y.-H. Kim, "Gate- versus defect-induced voltage drop and negative differential resistance in vertical graphene heterostructures," *Npj Comput. Mater.,* vol. 8, no. 1, 2022.

[5] L. Britnell *et al.*, "Resonant tunnelling and negative differential conductance in graphene transistors," *Nat. Commun.,* Article vol. 4, p. 1794, 04/30/online 2013.

[6] R. M. Feenstra, D. Jena, and G. Gu, "Single-particle tunneling in doped graphene-insulator-graphene junctions," *J. Appl. Phys.,* vol. 111, no. 4, p. 043711, 2012.

[7] J. Lee, H. Yeo, and Y.-H. Kim, "Quasi-Fermi level splitting in nanoscale junctions from ab initio," *Proc. Natl. Acad. Sci. U. S. A.,* vol. 117, no. 19, pp. 10142-10148, May 12 2020.

[8] J. Lee, H. S. Kim, and Y.-H. Kim, "Multi-space excitation as an alternative to the Landauer picture for nonequilibrium quantum transport," *Adv. Sci.,* vol. 7, no. 16, p. 2001038, Aug 2020.

[9] J. M. Soler *et al.*, "The SIESTA method for *ab Initio* order-N materials simulation," *J. Phys. Condens. Matter,* vol. 14, no. 11, pp. 2745-2779, 2002.

[10] D. M. Ceperley and B. J. Alder, "Ground state of the electron gas by a stochastic method," *Phys. Rev. Lett.,* vol. 45, no. 7, pp. 566-569, 08/18/ 1980.

[11] N. Troullier and J. L. Martins, "Efficient pseudopotentials for plane-wave calculations," *Phys. Rev. B,* vol. 43, no. 3, pp. 1993-2006, 01/15/ 1991.

[12] Y.-H. Kim, S. S. Jang, Y. H. Jang, and W. A. Goddard, III, "First-principles study of the switching mechanism of [2]catenane molecular electronic devices," *Phys. Rev. Lett.,* vol. 94, no. 15, p. 156801, Apr 22 2005.

[13] Y.-H. Kim, J. Tahir-Kheli, P. A. Schultz, and W. A. Goddard, III, "First-principles approach to the charge-transport characteristics of monolayer molecular-electronics devices: application to hexanedithiolate devices," (in English), *Phys. Rev. B,* vol. 73, no. 23, p. 235419, Jun 2006.

[14] S. Datta, *Electronic transport in mesoscopic systems*. Cambridge University Press: Cambridge, UK: Cambridge Univ. Press, New York, 1995. Cambridge University Press, Cambridge, UK.

[15] H. S. Kim, G. I. Lee, H. S. Kim, J. K. Kang, and Y.-H. Kim, "Intrinsically low-resistance carbon nanotube-metal contacts mediated by topological defects," *MRS Commun.,* vol. 2, no. 3, pp. 91-96, 2012.

[16] B.-K. Kim *et al.*, "Origins of genuine Ohmic van der Waals contact between indium and MoS2," *npj 2D Mater. Appl.,* vol. 5, no. 1, p. 9, 2021.